Zhang *et al. Chin. J. Mech. Eng.* (2020) 33:30
https://doi.org/10.1186/s10033-020-00445-3

Chinese Journal of Mechanical Engineering

ORIGINAL ARTICLE

Open Access

Analysis of Power Matching on Energy Savings of a Pneumatic Rotary Actuator Servo-Control System

Yeming Zhang[1*], Hongwei Yue[1], Ke Li[2] and Maolin Cai[3]

Abstract

When saving energy in a pneumatic system, the problem of energy losses is usually solved by reducing the air supply pressure. The power-matching method is applied to optimize the air-supply pressure of the pneumatic system, and the energy-saving effect is verified by experiments. First, the experimental platform of a pneumatic rotary actuator servo-control system is built, and the mechanism of the valve-controlled cylinder system is analyzed. Then, the output power characteristics and load characteristics of the system are derived, and their characteristic curves are drawn. The employed air compressor is considered as a constant-pressure source of a quantitative pump, and the power characteristic of the system is matched. The power source characteristic curve should envelope the output characteristic curve and load characteristic curve. The minimum gas supply pressure obtained by power matching represents the optimal gas supply pressure. The comparative experiments under two different gas supply pressure conditions show that the system under the optimal gas supply pressure can greatly reduce energy losses.

Keywords: Pneumatic rotary actuator, Energy savings, Gas supply pressure, Characteristic curve, Power matching

1 Introduction

The problem of energy shortages has become increasingly significant with the rapid development of society. In addition to discovering new energy sources, energy conservation is the most effective and important measure to fundamentally solve the energy problem [1]. Energy saving has increasingly become a hot topic of concern. Energy has always been a constraint to economic development, which makes energy-saving research more urgent and practical [2]. Currently, pneumatic technology is widely used in various fields of industry, and has become an important technical means of transmission and control [3, 4]. The use of existing technology to improve the energy utilization rate of energy-consuming equipment is an important energy-saving method [5].

However, the energy efficiency of pneumatic technology is relatively low [6]. Therefore, improving the efficiency of energy utilization and reducing the energy loss of pneumatic systems have become the concern of scholars all over the world [7, 8].

Pneumatic systems have three aspects of energy wastage [9, 10]: (1) gas and power losses during compressor gas production, (2) pressure loss in the gas supply pipeline, and (3) gas leakage from the gas equipment [11]. Accordingly, many methods are available to solve these problems. For the pressure loss in the air source, the timing of opening and closing of multiple air compressors can be optimized, and the gas production process of the air compressors can also be optimized, such as making full use of the expansion of compressed air to reduce unnecessary power consumption [12]. In order to reduce pressure loss in the pipeline, the method of reducing the pressure in the gas supply pipeline can be adopted [13]. When necessary, a supercharger can be added in front of the terminal equipment. For gas leakage from the gas equipment, optimizing the component

*Correspondence: zym@hpu.edu.cn
[1] School of Mechanical and Power Engineering, Henan Polytechnic University, Jiaozuo 454000, China
Full list of author information is available at the end of the article

structure is usually implemented to solve this problem. The pneumatic servo-control system precisely controls the angle of rotation; however, energy loss still occurs in the system. For this system, reducing the gas supply pressure is the most effective way of reducing the energy loss. Determining the critical pressure and reducing the gas supply pressure as much as possible while ensuring normal operation of the system are the key. The power-matching method can solve the optimization problem of the gas supply pressure based on the power required by the system [14]. In flow compensation, different compensation controllers can also be designed to match the flow and the system to realize the purpose of energy savings [15, 16]. Problems arise with regard to the high energy consumption and poor controllability of the rotary system of a hydraulic excavator due to throttle loss and overflow loss in the control valve during frequent acceleration and deceleration with large inertia. Therefore, Huang et al. [17] proposed the flow matching of a pump valve joint control and an independent measurement method of the hydraulic excavator rotary system to improve the energy efficiency of the system and reduce throttle loss. Xu et al. [18] designed a dynamic bypass pressure compensation circuit of a load sensing system, which solved the problems of pressure shock and energy loss caused by excessive flow and improved the efficiency and controllability of the system. Kan et al. [19] analyzed the basic characteristics of a hydraulic transmission system for wheel loaders using numerical calculation and adopted the optimal design method of a power-matching system. This improved the efficient working area of the system and average efficiency in the transportation process, and reduced the average working fuel consumption rate. Yang et al. designed an electro-hydraulic flow-matching controller with shunt ability to improve the dynamic characteristics and energy-saving effect and improve the stability of the system [20]. Guo et al. [21] used genetic algorithm to optimize the parameters of an asynchronous motor to achieve energy savings and consumption reduction, which proved the effectiveness and practicability of the power matching method of an electric pump system. Wang et al. [22] matched an engine and a generator to achieve efficiency optimization and obtained a common high efficiency area. They proposed a partial power tracking control strategy. Lai et al. [23] proposed a parameter matching method for an accumulator in a parallel hydraulic hybrid excavator and optimized the parameter matching process of the main components such as the engine, accumulator, and hydraulic secondary regulatory pump using genetic algorithm to reduce the installed power. Yan et al. [24] focused on the problem in which the flow of a constant displacement pump could not match with the changing load, resulting in energy loss. They proposed an electro-hydraulic flow-matching steering control method, which used a servo motor to drive a constant displacement pump independently to reduce the energy consumption of the system. At present, many studies on energy savings are conducted using the power matching method in the hydraulic system, but only few focus on the pneumatic system [25].

In the present study, a method of reducing the gas supply pressure is implemented to reduce energy loss of a pneumatic rotary actuator servo-control system. The output and load characteristic curves of the system are derived, and the power source characteristic curve is matched to determine the optimal gas supply pressure. Finally, the experiment verifies the energy-saving effect under this gas supply pressure.

Through theoretical analysis and experimental verification of the application platform of the pneumatic rotary actuator, a method of function matching and energy optimization method for the pneumatic rotary actuator under normal working conditions is proposed for the first time.

2 Experimental Platform

Figure 1 shows the schematic diagram of the pneumatic rotary actuator servo-control system.

As a gas source, the air compressor provides power to the system. The air filter, air regulator, and air lubricator are used to filter and clean the gas. When the driving voltage signal of the proportional directional control valve is given, the proportional valve controls the flow and direction of the gas, and then controls the rotary motion of the pneumatic rotary actuator. The rotary encoder measures the angular displacement and transmits the TTL (Transistor–Transistor Logic) level signals to the data acquisition card. The data acquisition card is installed in the industrial personal computer which calls the program of the upper computer, samples the encoder signal, and outputs a 0–10 V voltage signal through the controller calculation. The driving voltage signal output by the controller further regulates the flow and direction of the proportional directional control valve to reduce the angle error. After continuous iteration, the angle error of the system decreases and tends to stabilize.

Figure 2 shows the experimental platform of the pneumatic rotary actuator servo-control system. The round steel passes through the pneumatic rotary actuator and is connected to the rotary encoder through the coupling. The pneumatic rotary actuator is horizontally installed.

By selecting the MPYE-M5-010-B model proportional valve with a smaller range, we can more easily ensure the control accuracy of the system. The SMC MSQA30A pneumatic rotary actuator is adopted. The actuator has a high-precision ball bearing and belongs

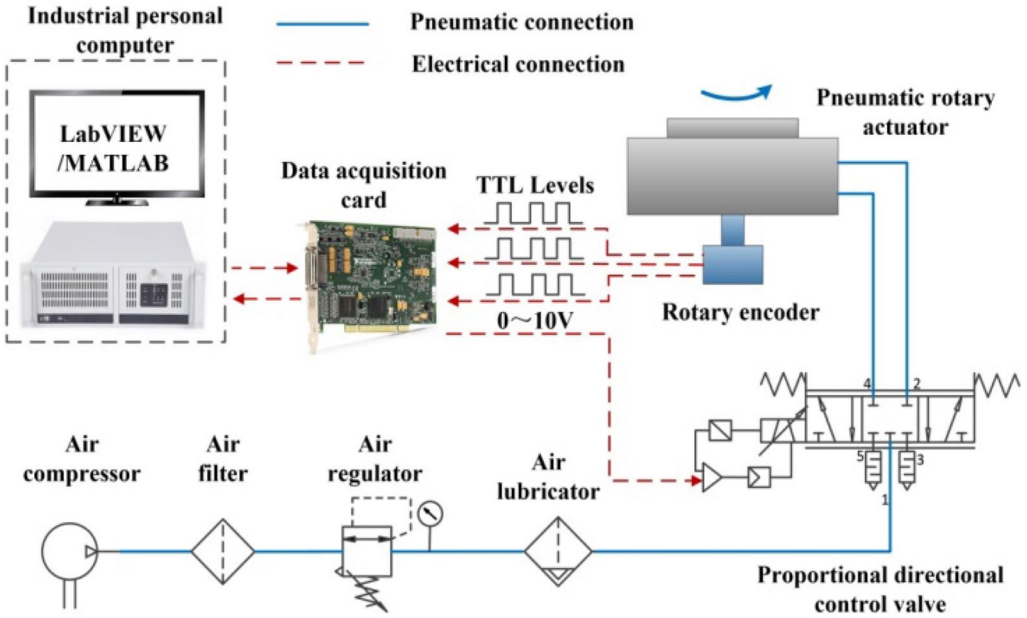

Figure 1 Schematic diagram of the pneumatic rotary actuator servo-control system

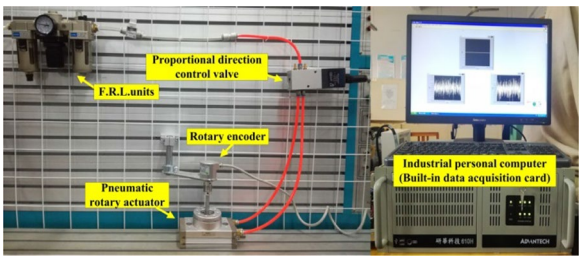

Figure 2 Experimental diagram of the pneumatic rotary servo-control system

to a high-precision actuator type. The rotating platform of the actuator contains many symmetrical threaded holes for easy introduction of loads. A high-precision rotary encoder is used, and the 20000P/R resolution corresponds to an accuracy of 1.8×10^{-2}°, which satisfies the high-precision measurement for the rotation angle. In addition, the air compressor and the filter, regulator, and lubricator (F. R. L.) units satisfy the gas supply pressure of at least 0.8 MPa. The digital I/O port and analog output port of the data-acquisition card must meet the experimental requirements, and the higher digit counter in the data-acquisition card improves the system response speed. The models and parameters of the components are listed in Table 1.

In some experimental tests, measuring the flow rate, pressure, and temperature of the gas is necessary, which can be performed using a flow sensor, a pressure transmitter, and a temperature transmitter (thermocouple), respectively. The flow rate in the inlet and outlet is measured using a flow sensor in the FESTO SFAB series

Table 1 Models and parameters of the components

Component	Model	Parameter
Air compressor	PANDA 750-30L	Maximum supply pressure: 0.8 MPa
F. R. L. units	AC3000-03	Maximum working pressure: 1.0 MPa
Proportional-directional control valve	FESTO MPYE-5-M5-010-B	3-position 5-way valve, 0–10 V driving voltage
Pneumatic rotary actuator	SMC MSQA30A	Bore: 30 mm; stroke: 190°
Rotary Encoder	GSS06-LDH-RAG20000Z1	Resolution: 20000P/R
Data-acquisition card	NI PCI-6229	32-bit counter; from − 10 V to + 10 V output voltage
Industrial personal computer	ADVANTECH IPC-610H	Standard configuration

with a range of 2–200 L/min, and the flow rate of the leak port is measured using a flow sensor with a range of 0.1–5 L/min in the SFAH series. The MIK-P300 pressure transmitter has high accuracy and fast response and can accurately measure the pressure changes. A thermocouple is used as a temperature transmitter to measure the gas temperature. To prevent signal interference, a temperature isolator is added to the circuit for the temperature signal transmission. The models and parameters of the test components are listed in Table 2. The circuit connection of the experimental platform is shown in Figure 3.

The schematic diagram of the valve-controlled cylinder system is constructed according to the experimental platform, as shown in Figure 4. The system consists of Chamber **a** and Chamber **b**. The dashed lines represent the boundaries of the chambers. Figure 4 shows the gas-flow mechanism when the spool moves to the right, and $\dot{m}_a$, $\dot{m}_b$ represent the mass flow rates of Chamber **a** and Chamber **b**, respectively. p_a, p_b and T_a, T_b represent the corresponding pressure and temperature of Chamber **a** and Chamber **b**, respectively. p_s is the gas supply pressure, p_e is the atmospheric pressure, and θ is the rotation angle of the pneumatic rotary actuator.

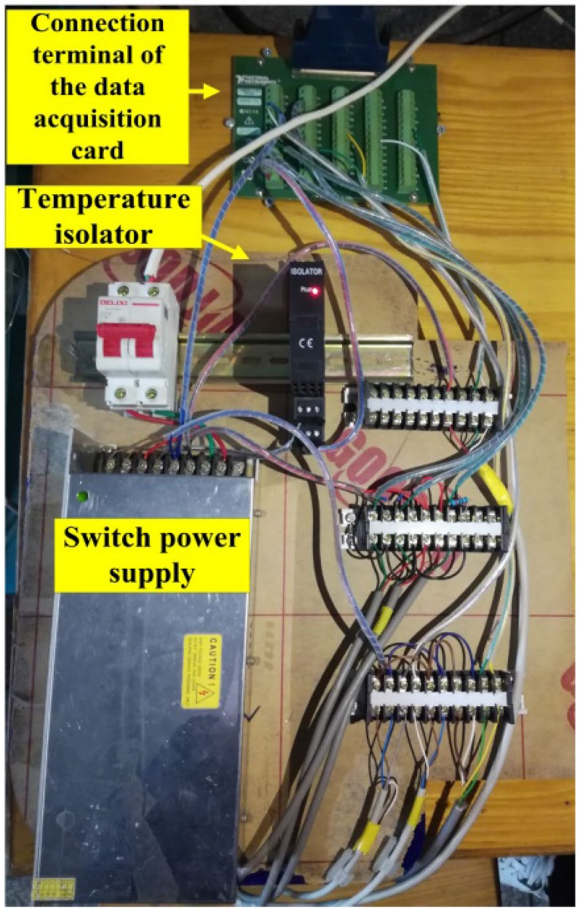

Figure 3 Circuit connection of the experimental platform

3 Power Characteristic Matching

3.1 Output Characteristics of the Valve-Controlled Cylinder

The output characteristic of the valve-controlled cylinder system refers to the relationship between the total load moment and angular velocity when the power source is known. The output characteristic can be obtained by the following method.

When supply pressure p_s is relatively low, i.e., when 0.1013 MPa $\leq p_s \leq$ 0.4824 MPa, the condition is satisfied, i.e., $p_a/p_s > b = 0.21$, where b denotes the critical pressure ratio. The gas flow in the proportional–directional control valve is a subsonic flow. Here, the mass flow equation through the proportional valve is [26]

$$\dot{m}_a = \frac{S_e p_s}{\sqrt{RT_s}} \sqrt{\frac{2\kappa}{\kappa - 1}\left[\left(\frac{p_a}{p_s}\right)^{\frac{2}{\kappa}} - \left(\frac{p_a}{p_s}\right)^{\frac{\kappa+1}{\kappa}}\right]}, \quad (1)$$

$$\dot{m}_b = \frac{S_e p_b}{\sqrt{RT_s}} \sqrt{\frac{2\kappa}{\kappa - 1}\left[\left(\frac{p_e}{p_b}\right)^{\frac{2}{\kappa}} - \left(\frac{p_e}{p_b}\right)^{\frac{\kappa+1}{\kappa}}\right]}, \quad (2)$$

Table 2 Models and parameters of the test components

Component	Model	Parameter
Pressure transmitter	MIK-P300	Range: 0–1.0 MPa; accuracy: 0.3% FS
Flow sensor 1	FESTO SFAB-200U-HQ8-2SV-M12	Range: 2–200 L/min; accuracy: 3% o.m.v. + 0.3% FS
Flow sensor 2	FESTO SFAH-5U-Q6S-PNLK-PNVBA-M8	Range: 0.1–5 L/min; accuracy: 2% o.m.v. + 1% FS
Temperature transmitter (thermocouple)	TT-K-36 (K type, diameter: 0.1 mm)	Range: 0–260°; accuracy: 0.4% FS
Temperature isolator	SLDTR-2P11	Response time: ≤ 10 ms; accuracy: 0.1% FS

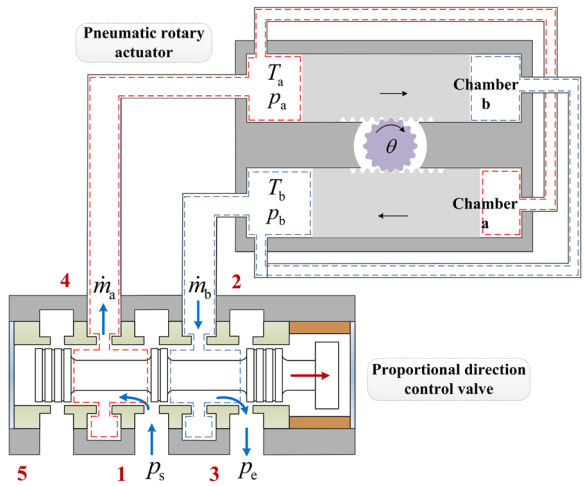

Figure 4 Schematic diagram of the valve-controlled cylinder system

where S_e is the effective area of the proportional valve orifice, R is the gas constant, T_s is the gas supply temperature, and κ is the isentropic index.

When the opening of the proportional–directional control valve is maximum, the mass flow rates of the two chambers are maximum, which can be expressed as

$$\dot{m}_{\text{a-max}} = \frac{C\pi r^2 p_s}{\sqrt{RT_s}}\sqrt{\frac{2\kappa}{\kappa-1}\left[\left(\frac{p_a}{p_s}\right)^{\frac{2}{\kappa}} - \left(\frac{p_a}{p_s}\right)^{\frac{\kappa+1}{\kappa}}\right]}, \tag{3}$$

$$\dot{m}_{\text{b-max}} = \frac{C\pi r^2 p_b}{\sqrt{RT_s}}\sqrt{\frac{2\kappa}{\kappa-1}\left[\left(\frac{p_e}{p_b}\right)^{\frac{2}{\kappa}} - \left(\frac{p_e}{p_b}\right)^{\frac{\kappa+1}{\kappa}}\right]}, \tag{4}$$

where C is the flow coefficient and r is the radius of the orifice.

Under adiabatic condition, $p_a/\rho_a^{\kappa} = p_s/\rho_s^{\kappa}$ and $p_b/\rho_b^{\kappa} = p_c/\rho_c^{\kappa}$, where ρ_a, ρ_b, ρ_s, and ρ_e represent the gas density in Chamber **a**, gas density in Chamber **b**, gas supply density, and atmospheric density respectively. For the pneumatic rotary actuator, these can be obtained from the mass flow-rate formulas:

$$\dot{m}_{\text{a-max}} = \rho_a \cdot 2A \cdot \frac{1}{2}d_f\dot{\theta} = \frac{\rho_a}{\rho_s}\rho_s A d_f\dot{\theta} = \left(\frac{p_a}{p_s}\right)^{\frac{1}{\kappa}}\frac{p_s}{RT_s}Ad_f\dot{\theta}, \tag{5}$$

$$\dot{m}_{\text{b-max}} = \rho_b \cdot 2A \cdot \frac{1}{2}d_f\dot{\theta} = \frac{\rho_e}{\rho_b}\rho_b A d_f\dot{\theta} = \left(\frac{p_e}{p_b}\right)^{\frac{1}{\kappa}}\frac{p_b}{RT_s}Ad_f\dot{\theta}, \tag{6}$$

where A is the effective area of a single piston, d_f is the pitch diameter of the gear, and $\dot{\theta}$ is the angular velocity of the pneumatic rotary actuator.

Table 3 Known parameters in Eq. (8)

Parameter	Value
A (m^2)	3.4636×10^{-4}
d_f (m)	0.014
κ	1.4
C	0.6437
r (m)	1.00×10^{-3}
R (J/(kg·K))	287

The dynamic equation of the pneumatic rotary actuator can be expressed as follows:

$$p_a - p_b = \frac{f}{d_f A}, \tag{7}$$

where f is the total load moment.

Combining Eqs. (3)–(6) yields p_a and p_b. Substituting the expressions of p_a and p_b into Eq. (7) yields

$$p_s\left[1 - \frac{A^2 d_f^2\dot{\theta}^2(\kappa-1)}{2C^2\pi^2 r^4\kappa RT_s}\right]^{\frac{\kappa}{\kappa-1}} - \frac{p_e}{\left[1 - \frac{A^2 d_f^2\dot{\theta}^2(\kappa-1)}{2C^2\pi^2 r^4\kappa RT_s}\right]^{\frac{\kappa}{\kappa-1}}} = \frac{f}{d_f A}. \tag{8}$$

Eq. (8) is the expression of the output characteristic curve of the valve-controlled cylinder. The known parameters in the equation are shown in Table 3.

To extend and improve the influence of the output characteristics of the system, the influence law of the fixed parameters is also theoretically analyzed. Figure 5 shows the output characteristic curves. The following characteristics can be found in plane $\dot{\theta}-f$:

(1) Figure 5(a) shows that when pressure p_s increases from 0.3 MPa to 0.4 MPa, the curve is a parabola and p_s is a variable parameter. Increasing p_s makes the whole parabola move to the right while the shape does not change.
(2) Figure 5(b) shows that when the maximum opening area of the valve increases from πr^2 to $2\pi r^2$, the whole parabola becomes wider but the vertices remain the same.
(3) Figure 5(c) shows that the increase in effective working area A of the piston makes the top of the parabola move to the right and the parabola simultaneously becomes narrower.

We can see from Eq. (8) that when $\dot{\theta}=0$, the maximum total load moment can be expressed as

$$f_{\max} = Ad_f(p_s - p_e). \tag{9}$$

When $f=0$, the maximum angular velocity is

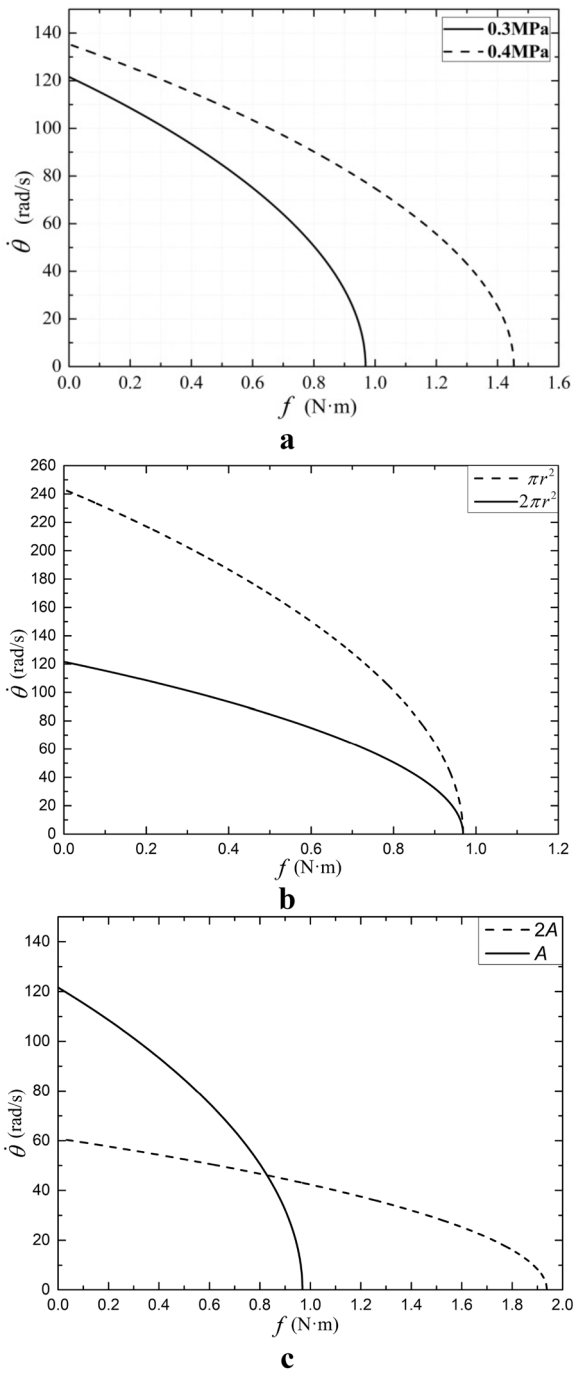

Figure 5 Output characteristic curve of the valve-controlled cylinder: (**a**) Output characteristics of the pressure variation, (**b**) Output characteristics of the change in the valve port area, (**c**) Output characteristics of the variation in the effective piston area

$$\dot{\theta}_{\max}=\sqrt{\frac{2C_1^2\pi^2r^4\kappa RT_s}{A^2d_f^2(\kappa-1)}\left[1-\left(\frac{p_e}{p_s}\right)^{\left(\frac{\kappa-1}{2\kappa}\right)}\right]}. \tag{10}$$

3.2 Load Characteristic

The load characteristic refers to the relationship between the moment required for the load to move and the position, velocity, and acceleration of the load itself [27]. The load characteristic can be expressed by the angular velocity–moment curve.

The load characteristic is related to the form of load movement. When the load sinusoidally moves, the motion of the load is expressed as

$$\theta=\theta_m\sin\omega t, \tag{11}$$

where θ_m is the maximum angular value of the load motion and ω is the sinusoidal motion frequency of the load.

The angular velocity and acceleration of the load are

$$\dot{\theta}=\theta_m\omega\cos\omega t, \tag{12}$$

$$\ddot{\theta}=-\theta_m\omega^2\sin\omega t. \tag{13}$$

The total load moment of the pneumatic rotary actuator is

$$\begin{aligned} f&=\left(\frac{1}{2}m_pd_f^2+J\right)\ddot{\theta}+\frac{1}{2}d_fF_f\\ &=-\left(\frac{1}{2}m_pd_f^2+J\right)\theta_m\omega^2\sin\omega t\\ &\quad+\frac{1}{2}d_f\left[F_c\mathrm{sign}(\dot{\theta})+(F_s-F_c)e^{-(\dot{\theta}/\dot{\theta}_s)^2}\mathrm{sign}(\dot{\theta})+\sigma\dot{\theta}\right], \end{aligned} \tag{14}$$

where m_p is the mass of a single piston and J is the moment of inertia of the pneumatic rotary actuator. F_f is the friction force and can be represented by the Stribeck friction model.

$$F_f=F_c\mathrm{sign}(\dot{\theta})+(F_s-F_c)e^{-(\dot{\theta}/\dot{\theta}_s)^2}\mathrm{sign}(\dot{\theta})+\sigma\dot{\theta}, \tag{15}$$

where F_s is the maximum static friction, F_c is the Coulomb friction, $\dot{\theta}_s$ is the critical Stribeck velocity, and σ is the viscous friction coefficient.

Table 4 Known parameters in Eq. (16)

Parameter	Value
F_s (N)	10.60
F_c (N)	6.03
$\dot{\theta}_s$ (rad/s)	0.19
σ (N·s/rad)	0.87
m_p (kg)	0.21

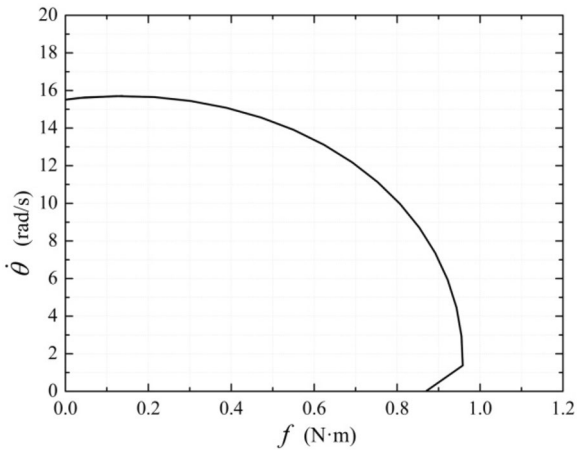

Figure 6 Load characteristic curve

Combining Eqs. (12)–(14) yields

$$\left[\frac{f-\frac{1}{2}d_f F_c \mathrm{sign}(\dot{\theta})-\frac{1}{2}d_f(F_s-F_c)e^{-(\dot{\theta}/\dot{\theta}_s)^2}\mathrm{sign}(\dot{\theta})}{\left(\frac{1}{2}m_p d_f^2+J\right)\theta_m\omega^2}-\frac{\frac{1}{2}d_f\sigma\dot{\theta}}{\left(\frac{1}{2}m_p d_f^2+J\right)\theta_m\omega^2}\right]^2+\left(\frac{\dot{\theta}}{\theta_m\omega}\right)^2=1. \tag{16}$$

The known parameters in Eq. (16) are listed in Table 4.

The load characteristic curve can be obtained from Eq. (16) when $\theta_m=180°$ and $\omega=10$ rad/s, as shown in Figure 6.

3.3 Power Source Characteristics and Matching

The power source characteristic refers to the characteristic of the flow and pressure provided by the power source, which can be expressed by the flow–pressure curve. The air compressor used in this work can be approximately regarded as a constant-pressure source for a quantitative pump. Therefore, the power source characteristic curve is shown in Figure 7, where $\dot{m}_s$ is the gas supply mass flow, p_s is the gas supply pressure, $\dot{m}_L$ is the driving mass flow, and p_L is the driving pressure.

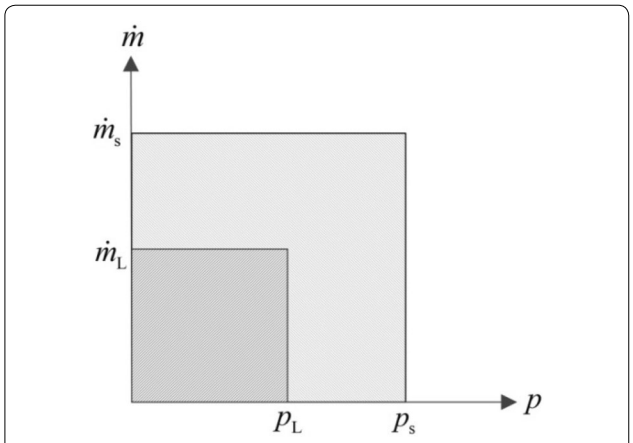

Figure 7 Power source characteristic curve

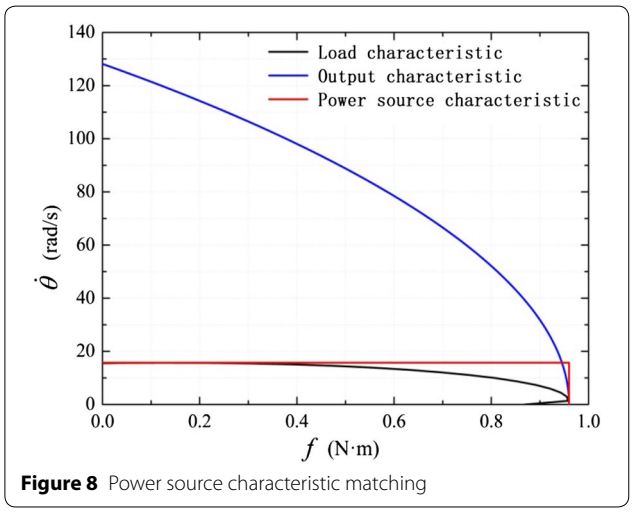

Figure 8 Power source characteristic matching

The output and power source characteristics of the valve-controlled cylinder should envelope the load characteristic curve. To minimize unnecessary energy consumption, the output characteristic curve should be tangent to the load characteristic curve, and the power source characteristic curve should be tangent to the output characteristic curve in the f-axis direction and the load characteristic curve in the $\dot{\theta}$-axis direction, as shown in Figure 8.

In this manner, the maximum total load moment is obtained, i.e., $f_{max}=0.96$ N·m. The optimum gas supply pressure can be obtained from Eq. (9), i.e., $p_s=f_{max}/d_f A+p_e=0.3367$ MPa.

4 Experimental Verification of the Energy Savings

To verify the calculation results presented in the previous section, low-speed uniform-motion experiments of the pneumatic rotary actuator were carried out using 0.6 and 0.3367 MPa supply pressure. The total energy and effective energy consumed by the valve-controlled cylinder system were measured and calculated. In the experiment, the input-angle signal was set as the slope signal, and Chamber **a** was used as the intake chamber. The motion curve of the uniform-velocity period was considered, and the angular strokes in the two experiments were the same. Two flow sensors were used to measure the volume flow of the gas supply pipeline and the Chamber **a** port. Temperature sensors were used to measure the gas temperature of the gas supply pipeline and Chamber **a**.

Figures 9 and 10 show the system response curves at gas supply pressure values of 0.6 and 0.3367 MPa, respectively, including the angle curve, gas supply flow curve, gas supply temperature curve, pressure curve of Chamber **a**, volume-flow curve of Chamber **a**, and temperature curve of Chamber **a**. Figures 9(f) and 10(f) show that the temperature in Chamber **a** changed with the change in the velocity, which first increased, then decreased, and then entered a stable stage.

The total power consumed by the pneumatic system is expressed as [28, 29]:

$$P_{\mathrm{T}} = p_{\mathrm{s}}\dot{V}_{\mathrm{s}}\left[\ln\frac{p_{\mathrm{s}}}{p_{\mathrm{e}}} + \frac{\kappa}{\kappa-1}\left(\frac{T_{\mathrm{s}}-T_{\mathrm{e}}}{T_{\mathrm{e}}} - \ln\frac{T_{\mathrm{s}}}{T_{\mathrm{e}}}\right)\right], \tag{17}$$

where $\dot{V}_{\mathrm{s}}$ is the volume flow through the gas supply pipeline, and its numerical variation curves are shown in Figures 9(b) and 10(b). The T_{s} curves are shown in Figures 9(c) and 10(c).

The effective power of the pneumatic rotary actuator can be expressed as

$$P_{\mathrm{E}} = p_{\mathrm{a}}\dot{V}_{\mathrm{a}}\left[\ln\frac{p_{\mathrm{a}}}{p_{\mathrm{e}}} + \frac{\kappa}{\kappa-1}\left(\frac{T_{\mathrm{a}}-T_{\mathrm{e}}}{T_{\mathrm{e}}} - \ln\frac{T_{\mathrm{a}}}{T_{\mathrm{e}}}\right)\right], \tag{18}$$

where $\dot{V}_{\mathrm{a}}$ is the volume flow into Chamber **a**, and its numerical variation curves are shown in Figures 9(e) and 10(e). The T_{a} curves are shown in Figures 9(f) and 10(f).

By substituting the data in Figures 9 and 10 into Eqs. (17) and (18), the total and effective power of the pneumatic system at different supply pressure values can be obtained, as shown in Figure 11. The total and effective energy consumed by the pneumatic system can be obtained by integrating the data shown in Figure 11 using the Origin software.

The actual work done by the gas on the pneumatic rotary actuator is equal to the sum of the rotational kinetic energy of the rotating platform, the kinetic energy of the cylinder piston, and the work done by the piston to overcome the friction force, which can be expressed as

$$\begin{aligned} \mathrm{W} &= \frac{1}{2}J\dot{\theta}^2 + \frac{1}{2}\cdot 2m_{\mathrm{p}}\cdot(\dot{y})^2 + F_{\mathrm{f}}y \\ &= \frac{1}{2}\left(J + \frac{1}{2}m_{\mathrm{p}}d_{\mathrm{f}}^2\right)\dot{\theta}^2 + \frac{1}{2}F_{\mathrm{f}}d_{\mathrm{f}}\theta, \end{aligned} \tag{19}$$

where y is the displacement of the actuator piston and $\dot{\theta}$ is replaced by the average value of the angular velocity.

The calculation results are described as follows. When the gas supply pressure is 0.6 MPa, the total energy consumed by the system is 195.552 J, the effective energy is 32.666 J, and the actual work done by the pneumatic rotary actuator is 3.513 J. When the gas supply pressure is 0.3367 MPa, the total energy consumed by the system is 32.207 J, the effective energy is 9.481 J, and the actual work done is 3.517 J. In both cases, the actual work of the pneumatic rotary actuator is almost the same, and when the gas supply pressure is 0.3367 MPa, the energy consumption is greatly reduced.

5 Further Discussions

According to the matching method of the power characteristics, for the constant-pressure source servo system with a quantitative pump, we need to calculate the optimal air-supply pressure required for manually adjusting the air-supply pressure to the optimal pressure. Matching efficiency η represents the ratio of the power output of the pneumatic system to the input power of the gas source. The matching efficiency is expressed as

$$\eta = \frac{p_{\mathrm{L}}\dot{m}_{\mathrm{L}}}{p_{\mathrm{s}}\dot{m}_{\mathrm{s}}}. \tag{20}$$

Figure 7 shows that the matching efficiency of this method is low. The adaptive power source can adaptively change the gas supply pressure or flow to meet the system requirements and improve the matching efficiency. It can be divided into the following three types [30].

(1) Flow adaptive power source

This power source can adaptively adjust the supply flow from the power source according to the system flow demand to reduce the loss in the flow. The characteristic curve is shown in Figure 12(a). The matching efficiency is expressed as

$$\eta = \frac{p_{\mathrm{L}}\dot{m}_{\mathrm{L}}}{p_{\mathrm{s}}\dot{m}'_{\mathrm{s}}} \approx \frac{p_{\mathrm{L}}}{p_{\mathrm{s}}}. \tag{21}$$

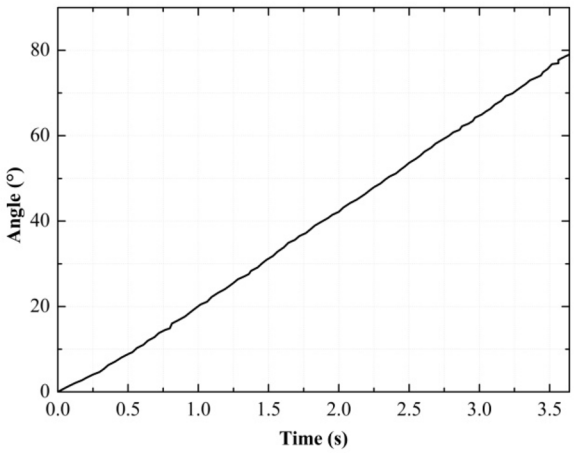

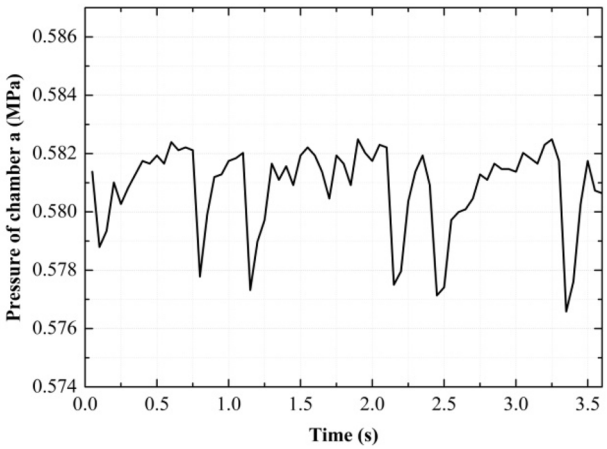

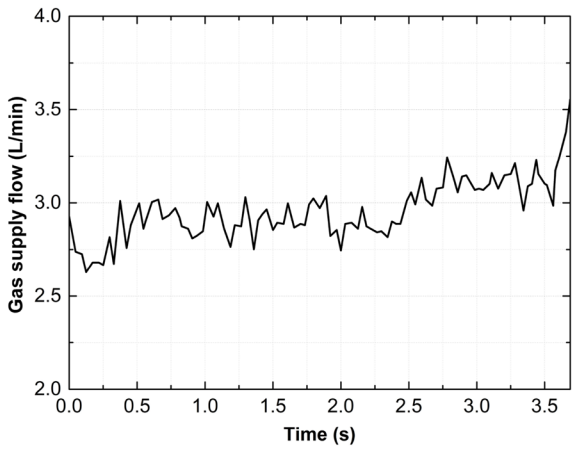

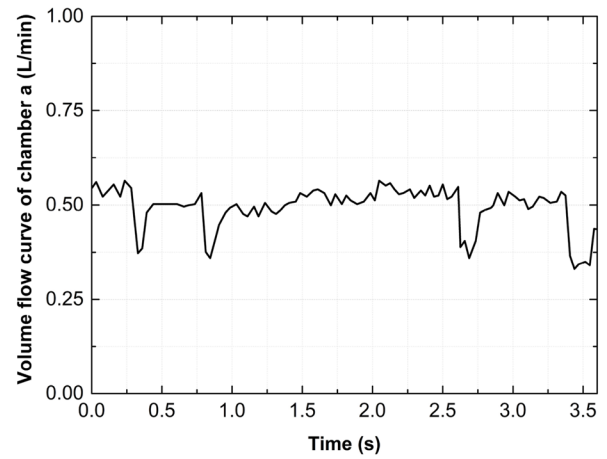

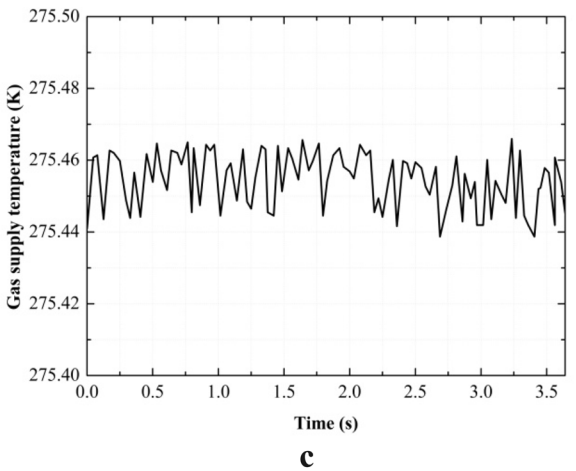

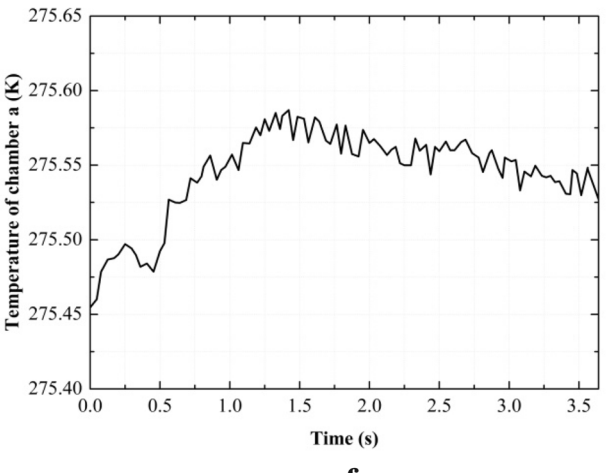

Figure 9 System-response curve at gas supply pressure of 0.6 MPa: (**a**) Angle curve, (**b**) Gas supply flow, (**c**) Gas supply temperature, (**d**) Pressure curve of Chamber **a**, (**e**) Volume-flow curve of Chamber **a**, (**f**) Temperature curve of Chamber **a**

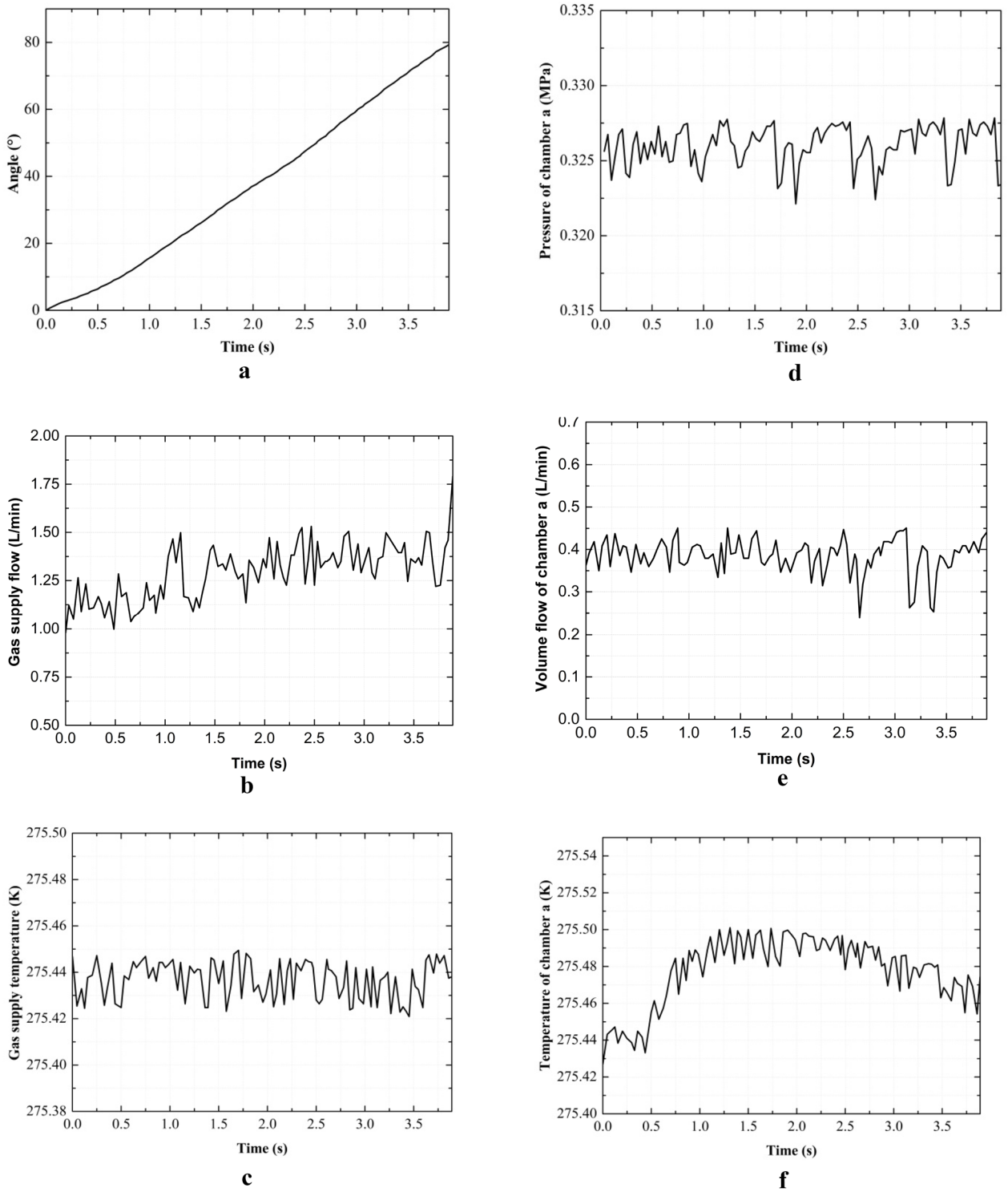

Figure 10 System response curve at gas supply pressure of 0.3367 MPa: (**a**) Angle curve, (**b**) Gas supply flow, (**c**) Gas supply temperature, (**d**) Pressure curve of Chamber **a**, (**e**) Volume-flow curve of Chamber **a**, (**f**) Temperature curve of Chamber **a**

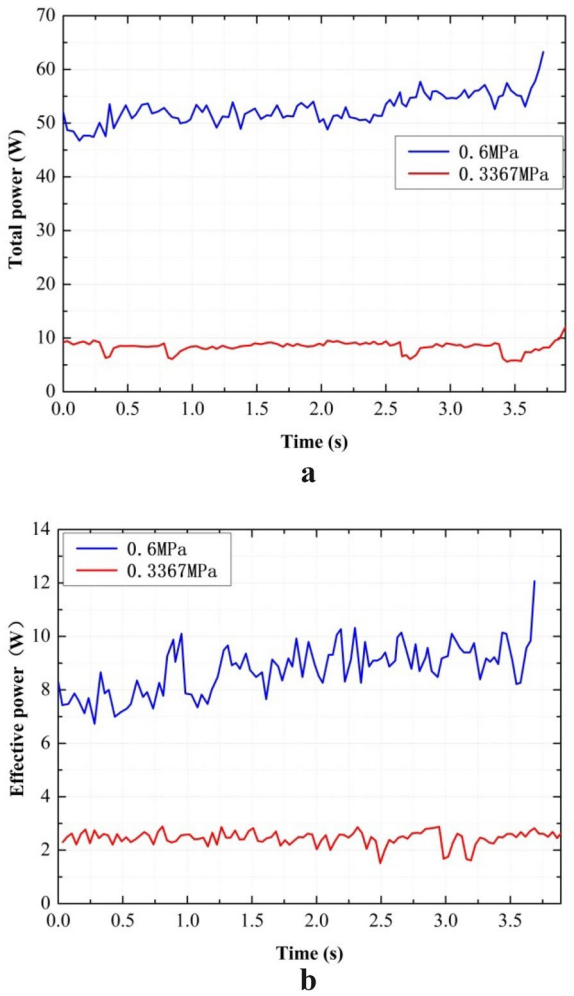

Figure 11 Total and effective power of the pneumatic system under different supply pressure values: (**a**) Total power, (**b**) Effective power

(2) Pressure adaptive power source

This power source can adaptively adjust the gas supply pressure of the power source according to the system pressure demand to reduce the pressure loss. The characteristic curve is shown in Figure 12(b). The matching efficiency is expressed as

$$\eta = \frac{p_{\mathrm{L}}\dot{m}_{\mathrm{L}}}{p_{\mathrm{s}}'\dot{m}_{\mathrm{s}}} \approx \frac{\dot{m}_{\mathrm{L}}}{\dot{m}_{\mathrm{s}}}. \tag{22}$$

(3) Power adaptive power source

This power source can adaptively adjust the gas supply pressure and flow from the power source according to the system pressure and flow demand to minimize the loss in power. $\dot{m}_{\mathrm{s}}^{'}$ denotes the air-supply flow. The characteristic

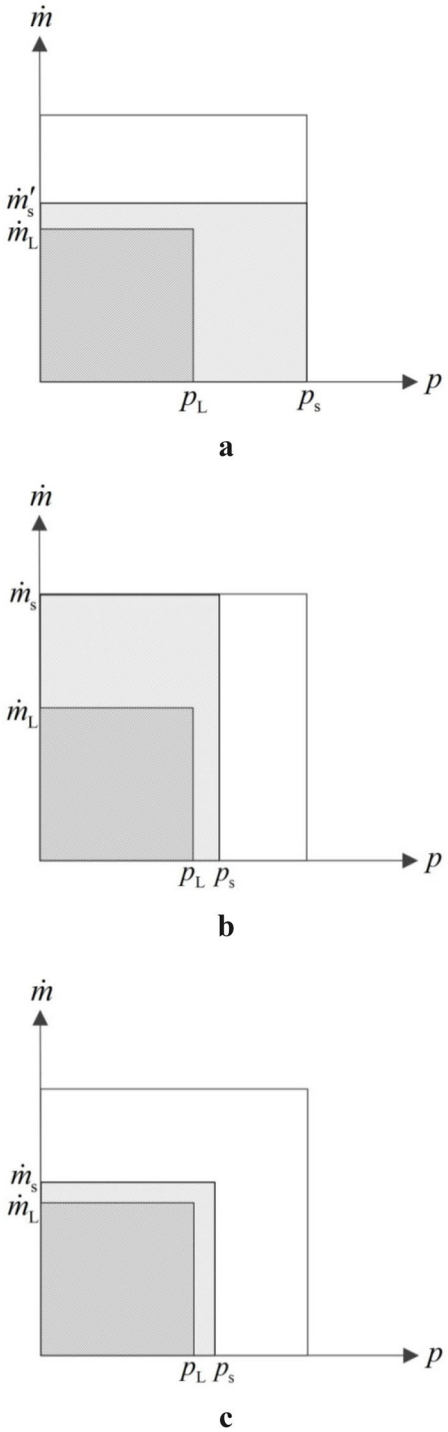

Figure 12 Power characteristics of the adaptive power sources: (**a**) Flow adaptive power source, (**b**) Pressure adaptive power source, (**c**) Power adaptive power source

curve is shown in Figure 12(c). The matching efficiency is expressed as

$$\eta = \frac{p_L \dot{m}_L}{p'_s \dot{m}'_s} \approx 1. \quad (23)$$

Therefore, the power adaptive power source demonstrates better energy-saving effect, and its matching efficiency is closer to 100%.

6 Conclusions

Power matching of the pneumatic rotary actuator involves optimizing the relevant parameters of the pneumatic rotary actuator system based on the premise of satisfying the normal operation of the pneumatic rotary actuator, realizing the power demand and output matching, and achieving energy savings. In this study, the derivation process of the output-power and load characteristics of the pneumatic rotary actuator servo-control system is described. The employed air compressor is regarded as a constant-pressure source of the quantitative pump, and the power characteristics of the system are matched. The following conclusions are obtained.

(1) The minimum gas supply pressure obtained by the power-matching method represents the optimal gas supply pressure. The optimum gas supply pressure is 0.3367 MPa.
(2) By comparing the system-response experiments at 0.6 and 0.3367 MPa, the total energy consumed by the system generates savings of 163.345 J. This value verifies that the system under the optimal gas supply pressure can significantly reduce energy loss.
(3) According to the characteristic curves of the adaptive power sources, the matching efficiency of the power adaptive power source is higher than that of the flow and pressure adaptive power sources.

Acknowledgments
The authors would like to thank Henan Polytechnic University and Beihang University for providing the necessary facilities and machinery to build the prototype of the pneumatic servo system. The authors are sincerely grateful to the reviewers for their valuable review comments, which substantially improved the paper.

Authors' Contributions
YZ provided guidance for the whole research. KL and HY established the model, designed the experiments and wrote the initial manuscript. KL and MC assisted with sampling and laboratory analyses. YZ and HY revised the manuscript, performed the experiments and analysed the data. All authors read and approved the final manuscript.

Authors' Information
Yeming Zhang, born in 1979, is currently is an associate professor at *School of Mechanical and Power Engineering, Henan Polytechnic University, China*. He received his PhD degree from *Beihang University, China*, in 2011. His research interests include complex mechatronics system design and simulation, intelligent control, reliability and fault diagnosis, pneumatic system energy saving and flow measurement.

Hongwei Yue, born in 1992, is currently a master candidate at *School of Mechanical and Power Engineering, Henan Polytechnic University, China*.

Ke Li, born in 1991, is currently a PhD candidate at *School of Mechanical and Electrical Engineering, Harbin Institute of Technology, China*. He received his master degree on mechano-electronic from *Henan Polytechnic University, China*, in 2019.

Maolin Cai, born in 1972, is currently a professor and a PhD candidate supervisor at *Beihang University, China*. He received his PhD degree from *Tokyo Institute of Technology, Japan*, in 2002. His main research direction includes pneumatic and hydraulic fluidics, compressed air energy storage, and pneumatic pipe line system.

Funding
Supported by Henan Province Science and Technology Key Project of China (Grant Nos. 202102210081, 202102210082), Fundamental Research Funds for Henan Province Colleges and Universities of China (Grant No. NSFRF140120), and Doctor Foundation of Henan Polytechnic University (Grant No. B2012-101).

Competing Interests
The authors declare no competing financial interests.

Author Details
[1] School of Mechanical and Power Engineering, Henan Polytechnic University, Jiaozuo 454000, China. [2] School of Mechanical and Electrical Engineering, Harbin Institute of Technology, Harbin 150001, China. [3] School of Automation Science and Electrical Engineering, Beihang University, Beijing 100191, China.

Received: 6 July 2019 Revised: 22 February 2020 Accepted: 18 March 2020
Published online: 09 April 2020

References

[1] L Ge, L Quan, X G Zhang, et al. Power matching and energy efficiency improvement of hydraulic excavator driven with speed and displacement variable power source. *Chinese Journal of Mechanical Engineering*, 2019, 32:100, https://doi.org/10.1186/s10033-019-0415-x.
[2] T Chen, L Cai, X F Ma, et al. Modeling and matching performance of a hybrid-power gas engine heat pump system with continuously variable transmission. *Building Simulation*, 2019, 12(2): 273-283.
[3] G W Jia, W Q Xu, M L Cai, et al. Micron-sized water spray-cooled quasi-isothermal compression for compressed air energy storage. *Experimental Thermal and Fluid Science*, 2018, 96: 470-481.
[4] D Shaw, J-J Yu, C Chieh. Design of a hydraulic motor system driven by compressed air. *Energies*, 2013, 6(7): 3149-3166.
[5] M Cheng, B Xu, J H Zhang, et al. Pump-based compensation for dynamic improvement of the electrohydraulic flow matching system. *IEEE Transactions on Industrial Electronics*, 2017, 64(4): 2903-2913.
[6] Y M Zhang, K Li, G Wang, et al. Nonlinear model establishment and experimental verification of a pneumatic rotary actuator position servo system. *Energies*, 2019, 12(6): 1096.
[7] T L Brown, V P Atluri, J P Schmiedeler. A low-cost hybrid drivetrain concept based on compressed air energy storage. *Applied Energy*, 2014, 134: 477-489.
[8] Y M Zhang, M L Cai. Overall life cycle comprehensive assessment of pneumatic and electric actuator. *Chinese Journal of Mechanical Engineering*, 2014, 27(3): 584-594.
[9] M L Cai. Energy saving technology on pneumatic systems. *Chinese Hydraulics & Pneumatics*, 2013(8): 1-8. (in Chinese)
[10] J F Li. *Energy saving of pneumatic system*. Beijing: Machinery Industry Press, 1997. (in Chinese)
[11] R Saidur, N A Rahim, M Hasanuzzaman. A review on compressed-air energy use and energy savings. *Renewable and Sustainable Energy Reviews*, 2010, 14(4): 1135-1153.
[12] Y M Zhang, S Wang, S L Wei, et al. Optimization of control method of air compressor group under intermittent large flow condition. *Fluid Machinery*, 2017, 45(7): 7-11.

[13] K Baghestan, S M Rezaei, H A Talebi, et al. An energy-saving nonlinear position control strategy for electro-hydraulic servo systems. *ISA Trans.*, 2015, 59: 268-279.
[14] S P Yang, H Yu, J G Liu, et al. Research on power matching and energy saving control of power system in hydraulic excavator. *Journal of Mechanical Engineering*, 2014, 50(5): 152-160. (in Chinese)
[15] M Cheng, B Xu, J H Zhang, et al. Valve-based compensation for controllability improvement of the energy-saving electrohydraulic flow matching system. *Journal of Zhejiang University: Science A*, 2017, 18(6): 430-442.
[16] B Xu, M Cheng, H Y Yang, et al. A hybrid displacement/pressure control scheme for an electrohydraulic flow matching system. *IEEE/ASME Transactions on Mechatronics*, 2015, 20(6): 2771-2782.
[17] W N Huang, L Quan, J H Huang, et al. Flow matching with combined control of the pump and the valves for the independent metering swing system of a hydraulic excavator. *Proceedings of the Institution of Mechanical Engineers, Part D: Journal of Automobile Engineering*, 2018, 232(10): 1310-1322.
[18] B Xu, M Cheng, H Y Yang, et al. Electrohydraulic flow matching system with bypass pressure compensation. *Journal of Zhejiang University (Engineering Science)*, 2015, 49(9): 1762-1767. (in Chinese)
[19] Y Z Kan, D Y Sun, Y Luo, et al. Optimal design of power matching for wheel loader based on power reflux hydraulic transmission system. *Mechanism and Machine Theory*, 2019, 137: 67-82.
[20] H Y Yang, W Liu, B Xu, et al. Characteristic analysis of electro-hydraulic flow matching control system in hydraulic excavator. *Journal of Mechanical Engineering*, 2012, 48(14): 156-163. (in Chinese)
[21] X Guo, C Lu, J Li, et al. Analysis of motor-pump system power matching based on genetic algorithm. *EEA - Electrotehnica, Electronica, Automatica*, 2018, 66(1): 93-99.
[22] X Wang, H Lv, Q Sun, et al. A proportional resonant control strategy for efficiency improvement in extended range electric vehicles. *Energies*, 2017, 10(2): 204.
[23] X L Lai, C Guan. A parameter matching method of the parallel hydraulic hybrid excavator optimized with genetic algorithm. *Mathematical Problems in Engineering*, 2013: 1-6.
[24] X D Yan, L Quan, J Yang. Analysis on steering characteristics of wheel loader based on electric-hydraulic flow matching principle. *Transactions of the Chinese Society of Agricultural Engineering*, 2015, 31(18): 71-78. (in Chinese)
[25] L C Xu, X M Hou. Power matching on loader engine and hydraulic torque converter based on typical operating conditions. *Nongye Gongcheng Xuebao/Transactions of the Chinese Society of Agricultural Engineering*, 2015, 31(7): 80-84. (in Chinese)
[26] X H Fu, M L Cai, W Y X ang, et al. Optimization study on expansion energy used air-powered vehicle with pneumatic-hydraulic transmission. *Chinese Journal of Mechanical Engineering*, 2018, 31:3, https://doi.org/10.1186/s10033-018-0220-y.
[27] H B Yuan, H Na, Y Kim. Robust MPC–PIC force control for an electro-hydraulic servo system with pure compressive elastic load. *Control Engineering Practice*, 2018, 79: 170-184.
[28] Y Shi, M L Cai, W Q Xu, et al. Methods to evaluate and measure power of pneumatic system and their applications. *Chinese Journal of Mechanical Engineering*, 2019, 32:42, https://doi.org/10.1186/s10033-019-0354-6.
[29] Y Shi, T C Wu, M L Cai, et al. Energy conversion characteristics of a hydro-pneumatic transformer in a sustainable-energy vehicle. *Applied Energy*, 2016, 171: 77-85.
[30] C C Zhan, X Y Chen. *Hydraulic reliability optimization and intelligent fault diagnosis*. Beijing: Metallurgical Industry Press, 2015. (in Chinese)